

Molecular dynamics study of the structure organization in a strongly coupled chain of charged particles

Motohiko Tanaka,¹ A. Yu Grosberg,^{2,*} V. S. Pande,^{2,3} and Toyochi Tanaka²

¹Research and Information Center, National Institute for Fusion Science, Toki 509-52, Japan

²Department of Physics and Center for Materials Science and Engineering, Massachusetts Institute of Technology, Cambridge, Massachusetts 02139

³Physics Department, University of California at Berkeley, Berkeley, California 94720

(Received 8 July 1997)

The dynamical and equilibrium properties of a strongly coupled chain of charged particles (polyampholyte) submerged in an immobile viscous medium are studied using the molecular dynamics simulations. The polyampholyte relaxes to an equilibrium conformation typically in $300\omega_{pe}^{-1}$ due to folding of the chain for low temperatures, and expands several times faster for high temperatures, where ω_{pe} is the plasma frequency. Three regimes with distinct conformations as stretched, oblate, and spherical are observed under the Coulomb force at high, medium, and low temperatures, respectively. The change in the conformations is considered to minimize the free energy through the electrostatic potential. The root-mean-squared size of the polyampholytes in these regimes is scaled, respectively, as $R_g \sim N^{1/2}$, $(NT)^{1/3}$, and $N^{0.3}T^{0.8-1.0}$, where N is the number of monomers on the chain and T the temperature. The crossover point of the regimes is characterized by the unique values of the monomer distance $2R_g/N^{1/3}$, being insensitive to the length and stiffness of the chain. The present results agree well with the Flory theory in the high and medium temperature regimes. The densely packed state at low temperatures is first obtained here without the use of the lattice model. The transition among the different regimes under the Coulomb force is exactly reversible. However, the transition under the cooperation of the Coulomb force and the attractive short-range force exhibits a hysteresis against successive changes in temperature. [S1063-651X(97)13111-7]

PACS number(s): 36.20.Ey, 52.25.Wz, 61.25.Hq, 64.60.Cn

I. INTRODUCTION

The strongly coupled Coulomb systems are found in condensed matter, highly compressed laser-irradiated plasmas, and the stellar interiors [1–3]. In these circumstances, the Coulomb interactions organize the structure of matter and determine their equilibrium properties. The polyampholyte to be studied in this paper is the charged chain that is composed of a random sequence of positive and negative monomers that have little net charges on the chain [4]. These monomers, which represent a group of atoms or molecules, are connected by the molecular binding force of the entropic elasticity type. The polyampholyte is an idealization of material gels and polymers [5,6], and proteins in biochemical systems [7]. Such polyampholytes are usually submerged in a viscous medium (solvent), which works as a thermal reservoir to exert random thermal forces and frictions on them.

The properties of the polyelectrolyte that is the chain of charged monomers of the same sign were extensively studied to theoretically understand dissolution of the homogeneously charged polymers in solvents [8] and physical behaviors of DNA [9]. However, the polyampholytes remained infrequently studied until quite recently because of their complexity due to inhomogeneity of the charge sequences. The first theoretical study of the polyampholytes using the Coulomb force can be found in Ref. [10]. Recently, the two-parametric

Flory theory was developed to explain both the polyelectrolyte and polyampholyte regimes of charged chains [11]. On the other hand, extensive numerical studies were performed by means of the Monte Carlo simulation with the lattice model [5] where static properties of the polyampholytes were examined using the energy principle to obtain the lower energy state.

For the polyampholytes, the number of charged monomers in the Debye sphere is typically not very large and may be as small as of the order of unity. This is why the polyampholyte chain is not considered a continuous medium, in sharp contrast with ordinary high temperature plasmas [12]. For this reason, the direct Coulomb interactions between the charged monomers play major roles in the structure organization, which need to be calculated with high accuracy in numerical computations. The dynamics of the polyampholyte chain with finite size monomers is governed by the electrostatic and thermal interactions, as characterized in the coupling constant $\Gamma = e^2/aT$, and also by the stiffness of the chain v/a^3 . Here, e is electron charge, a the monomer distance, v the volume of the monomer, and T the temperature in the energy unit ($k_B T$ if T is measured in degrees, with k_B the Boltzmann constant). We remark here that, since we are going to study the global structure of the polyampholytes as stated in the Introduction, it is reasonable to use classical mechanics, not including quantum mechanical effects.

Molecular dynamics (particle simulation), which is a tool adopted in this study, integrates Newton's equations of motion in time to trace the dynamical evolution of the N -body system. With the method, we are able to study dynamical

*On leave from the Institute of Biochemical Physics, Russian Academy of Sciences, Moscow 117977, Russia.

and equilibrium properties, including reaction and relaxation processes along the dynamical paths. The aforementioned Monte Carlo simulation with the lattice model [5] was useful in studying the static properties of flexible polymers with $v/a^3 \leq 1$. However, it did not include dynamical effects and may have eliminated the densely packed state of stiff polymers at low temperatures, which is presented in this study.

Therefore, the issues of the polyampholytes to be studied here by molecular dynamics simulations are the formation of equilibrium conformations and dynamical paths toward such states under the long-range Coulomb force and other short-range forces. Further, the dependence of the final equilibrium states on the initial conformations and randomness of the charge sequences is examined, as well as the reversibility of the transition among the equilibrium states that is invoked by temperature changes. The last issue relates to an existence of the metastable states or the local energy minima.

The outline of this paper is the following. In Sec. II, the equations used in the present molecular dynamics simulations are presented. We include (1) the long-range electrostatic (Coulomb) force, (2) the harmonic binding force between the adjacent monomers, and (3) the random thermal kicks and the frictional force originating from the surrounding medium. In Sec. III, we will examine the dynamics and equilibrium of a chain of charged N -body system. The relaxation to equilibrium conformations occurs in $(200-300) \omega_{pe}^{-1}$ due to folding of the chain, and the expansion at high temperatures is several times faster, where ω_{pe} is the plasma frequency. Three temperature regimes of the polyampholytes with different conformations and parameter dependences are observed. The free energy is minimized by the change in the conformations through the electrostatic potential. Good agreement between the molecular dynamics simulation and the Flory theory of the polyampholytes [11] is obtained in the high and medium temperature regimes. On the other hand, the densely packed compact state at low temperatures is discovered in the present study, which does not adopt the lattice model (Sec. III B). Then, in Sec. IV we add the short-range attractive force to find the cooperative effects of the long- and short-range forces. A hysteresis of the transition path among the equilibrium states is demonstrated. Section V will be the summary and conclusion of this paper.

II. EQUATIONS OF MOTION

For the purpose of studying the dynamical evolution and equilibrium properties of the polyampholytes [13], we solve the equations of motion for the positions and velocities of the N monomers. The equations for the i th monomer ($i = 1, \dots, N$) is written as

$$m \frac{d\mathbf{v}_i}{dt} = \mathbf{F}_{LR}(\mathbf{r}_i) - \frac{3T}{a^2} (2\mathbf{r}_i - \mathbf{r}_{i+1} - \mathbf{r}_{i-1}) + \mathbf{F}_{th} - \nu m \mathbf{v}_i, \quad (1)$$

$$\frac{d\mathbf{r}_i}{dt} = \mathbf{v}_i. \quad (2)$$

The electrostatic Coulomb force, which is a long-range force, is given by

$$\mathbf{F}_{LR}(\mathbf{r}_i) = \sum_j \frac{Z_i Z_j e^2}{|\mathbf{r}_i - \mathbf{r}_j|^2} \hat{\mathbf{r}}_{ij}. \quad (3)$$

Here, \mathbf{r}_i and \mathbf{v}_i are the position and velocity of the i th monomer, respectively, m , Z_i are mass and charge state ($Z_i = \pm 1$ is assumed), $\hat{\mathbf{r}}_{ij}$ is a unit vector along $(\mathbf{r}_i - \mathbf{r}_j)$, and ν is the friction constant. In Eq. (3), the Coulomb force is summed over all the possible monomer pairs, and the harmonic spring force connecting the monomers is calculated pairwise. The thermal force \mathbf{F}_{th} that acts on the monomers is generated using random numbers with a Gaussian distribution in each time step. The frictional constant ν is chosen such that the average kinetic energy of the monomers equals $3/2T$ [7]. The thermal and friction forces exerted by the surrounding medium serve to maintain the kinetic energy of the N -body system at the thermal equilibrium level.

It is emphasized that the monomers on the chain can occupy any point in the six-dimensional space (\mathbf{r}, \mathbf{v}) , unlike the lattice model [5]. This turns out to be important especially for the densely packed states in the low temperature regime to be presented in Sec. III, because the exclusion effect of the neighboring monomers becomes apparent in such states. The minimum distance allowed for any pair of monomers is $a_{col} = 0.2a$ or $0.5a$, below which the monomers are elastically scattered. The stiffness of the chain in our simulation then becomes $v/a^3 = (\pi/6)(a_{col}/a)^3 \sim 0.004 - 0.065$, where $v = (4\pi/3)(a_{col}/2)^3$ is the exclusion volume of the monomer. The chosen stiffness well represents those values obtained by laboratory experiments, i.e., $v/a^3 \leq 0.2$ for most flexible monomers, and $v/a^3 \sim 0.003$ for double helix DNA [7].

All the simulation quantities in Secs. III and IV are normalized as nondimensional ones (the quantities with carets):

$$\mathbf{r} = a \hat{\mathbf{r}}, \quad \mathbf{v} = a \omega_p \hat{\mathbf{v}}, \quad t = \hat{t} \omega_p^{-1}, \quad (4)$$

with $\omega_p = \sqrt{4\pi n_0 e^2 / m}$ being the plasma frequency and n_0 the initial number density of (positively) charged monomers. If we assume nearly neutral polyampholytes $n_0 a^3 \sim 1/2$, then we have $\omega_p \sim (2\pi e^2 / m a^3)^{1/2}$. For the CH_2 monomers with $a = 5 \text{ \AA}$ and $e = 0.1 \text{ esu}$, we have $\omega_p \sim 2 \times 10^{12} \text{ s}^{-1}$ ($\omega_p^{-1} \sim 0.5 \text{ ps}$) and the coupling constant $\Gamma \sim 1$ at room temperature. Under this normalization, the equations of motion are written as (the caret is suppressed hereafter)

$$\frac{d\mathbf{v}_i}{dt} = \mathbf{F}_{LR}(\mathbf{r}_i) - \frac{3}{4\pi\Gamma} (2\mathbf{r}_i - \mathbf{r}_{i+1} - \mathbf{r}_{i-1}) + \mathbf{F}_{th} - \xi \mathbf{v}_i, \quad (5)$$

$$\frac{d\mathbf{r}_i}{dt} = \mathbf{v}_i, \quad \mathbf{F}_{LR}(\mathbf{r}_i) = \frac{1}{4\pi} \sum_j \frac{Z_i Z_j}{|\mathbf{r}_i - \mathbf{r}_j|^2} \hat{\mathbf{r}}_{ij}. \quad (6)$$

We see in Eq. (5) two nondimensional parameters,

$$\Gamma = \frac{e^2}{aT}, \quad \xi = \frac{\nu}{\omega_p}. \quad (7)$$

The other important parameter is the exclusion length a_{col} , or the stiffness of the chain v/a^3 in the nondimensional form, which arises from geometrical exclusion of adjacent monomers. Γ is the so-called coupling constant, which is an inverse of temperature T . In high-temperature plasmas, the

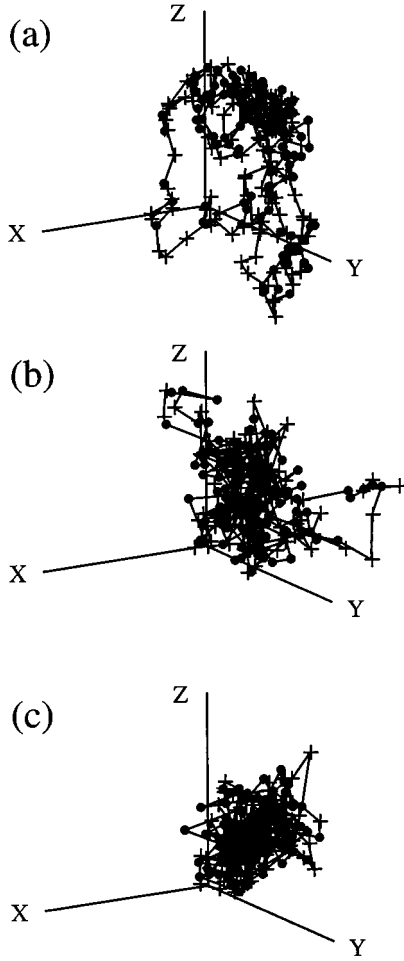


FIG. 1. The time sequential plots of the 256-mer polyampholyte chain at (a) $t=0$, (b) $t=50\omega_{pe}^{-1}$, and (c) $t=600\omega_{pe}^{-1}$ of molecular dynamics simulation. The parameters are $T=1/2T_0$, $a_{col}=0.2a$, and the charge imbalance is 1.6%. The + and dot on the chain represent positive and negative monomers, respectively.

condition $\Gamma \ll 1$ is always satisfied to ensure shielding of the electric field beyond the Debye length [12]. However, the Debye shielding is incomplete in the polymer system as the Debye sphere contains only few charged monomers.

III. DYNAMICAL AND EQUILIBRIUM PROPERTIES DUE TO THE COULOMB FORCE

A. Dependence on the charge imbalance

The temporal evolution of the polyampholyte chains and their equilibrium properties under the long-range Coulomb force are examined with various amounts of charge imbalance. The temperature for the run depicted in Fig. 1 is $T=1/2T_0$ (the coupling constant $\Gamma=e^2/aT=2$), the exclusion length is $a_{col}=0.2a$, and the friction constant is $\xi=0.1$, where the base temperature T_0 corresponds to $\Gamma_0=e^2/aT_0=1$. The net charge of this chain consisting of 256 randomly distributed charged monomers is 1.6%. In Fig. 1 and the following figures, the plusses and circles on the chain represent the positive and negative monomers, respectively. For the chosen parameters, the initial conformation in Fig. 1(a) is organized to be a spherical and compact globule

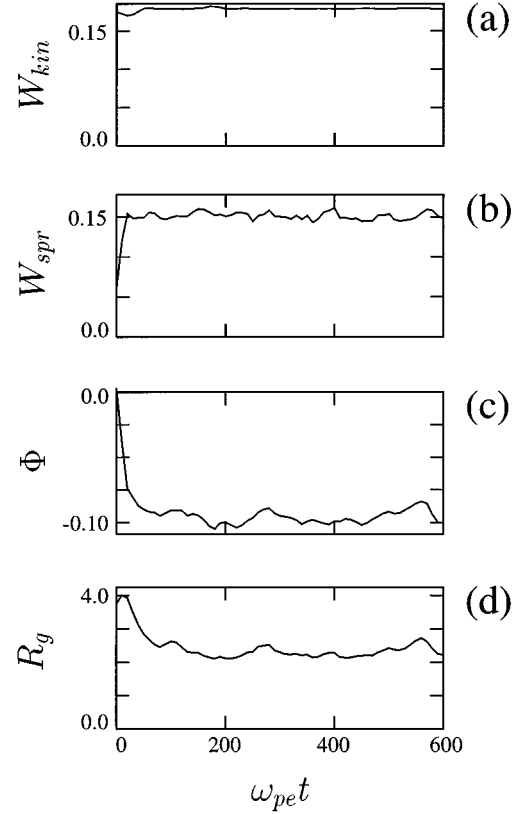


FIG. 2. The time histories of (a) the kinetic energy, (b) the elastic energy, (c) the electrostatic potential, and (d) the gyration radius (the root-mean-squared size) of the polyampholyte shown in Fig. 1.

in a few hundred times the inverse of the plasma frequency. The conformation at $\omega_{pe}t=50$ shown in Fig. 1(b) is already close to the final and equilibrium conformation of Fig. 1(c).

The time histories of the kinetic energy, the elastic (spring) energy, the electrostatic potential, and the gyration radius defined by

$$R_g = \left(\frac{1}{N} \sum_i (\mathbf{r}_i - \langle \mathbf{r} \rangle)^2 \right)^{1/2} \quad (8)$$

are depicted in Fig. 2 for the above polyampholyte chain, where $\langle \mathbf{r} \rangle$ stands for the gravity center of all the monomers. The average kinetic energy per monomer is held constant, $W_{kin} \sim 3/2T$, by the thermal kicks and the frictional force, as seen in Fig. 2(a). The elastic energy that is proportional to the mean square of the average distance between the connected monomers, $\langle (\Delta r)^2 \rangle$, increases quickly in the initial transient phase of $t \leq 20\omega_{pe}^{-1}$. Beyond this time, the energy equipartition is satisfied during the run, $W_{kin} \sim W_{spr}$. Also, the electrostatic potential and the radius relax to equilibrium values, whose relaxation (e -folding) time $\tau_{rel} \sim 280\omega_{pe}^{-1}$ is long compared to that of the elastic energy. Oscillating fluctuations with $\tau_{N=256} = (130 - 170)\omega_{pe}^{-1}$ are observed for $N=256$ in Figs. 2(c) and 2(d), whereas the oscillation period for $N=64$ is $\tau_{N=64} \sim 80\omega_{pe}^{-1}$. The oscillation period is pro-

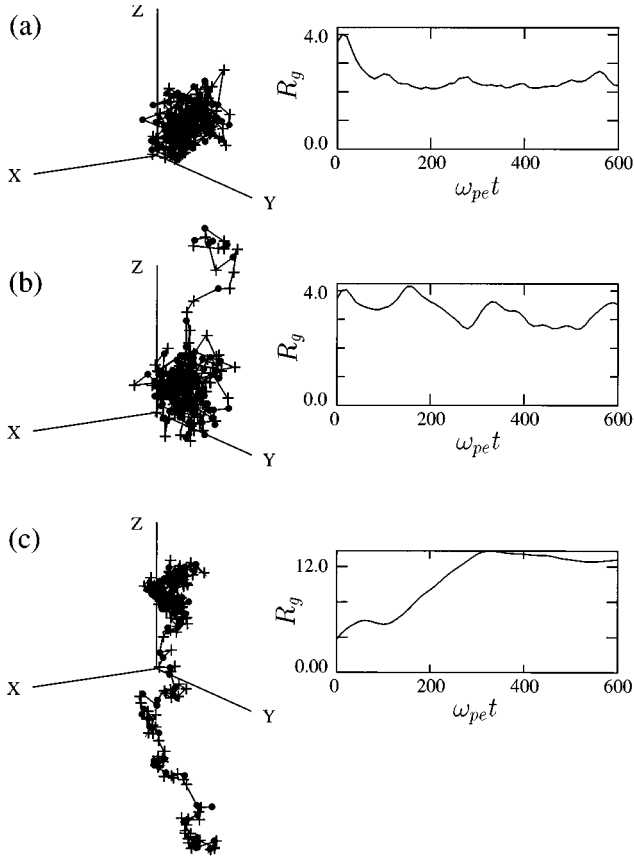


FIG. 3. The equilibrium conformations and the time histories of the gyration radius for the 256-mer chains with $a_{\text{col}}=0.2a$ and $T=\frac{1}{2}T_0$. The charge imbalance is (a) $\delta N/N=1.6\%$, (b) 6.3% , and (c) 14.1% . The conformation for (c) is reduced to 53% that of the real size.

portional to \sqrt{N} , implying that the mass (length) of the oscillating arm (a part of the chain) is proportional to the total mass (length) of the chain.

The observed two relaxation mechanisms in the short and long time scales, respectively, are the local adjustment of the connected monomer distances by elasticity, and the global structure organization due to folding of the chain under the Coulomb force.

Figure 3 shows variability of the equilibrium conformations due to the charge imbalance and the time histories of the corresponding gyration radius for the 256-mer chains. The net charges are (a) $\delta N/N=1.6\%$, (b) 6.3% , and (c) 14.1% . [The scale of the three-dimensional plot (c) is reduced to about half the real size.] The chain collapses to $R_g \sim 2.3a$ for the small net charge case (a), but it swells to $R_g \sim 13a$ for the significantly non-neutral case (c). The equilibrium conformation for the small net charge case is a spherical and compact globule. For this case, the attractive force by the elasticity that is provided by the harmonic springs overcomes the electrostatic repulsive force. The gyration radius for the case with intermediate charge imbalance in Fig. 3(b) undergoes amplitude oscillations whose period is $200\omega_{pe}^{-1}$. When the charge imbalance is larger, the gyration radius increases monotonically in time and the chain becomes highly stretched, as shown in Fig. 3(c). The relaxation

time of the structure for these 256-mers is $\tau_{\text{rel}} = (200 - 300)\omega_{pe}^{-1}$. The criterion for the collapse and expansion of the polyampholytes against the charge imbalance agrees with that obtained by the Monte Carlo simulation [5]. A simple theory based on the energy principle and valid for the non-neutral polyampholyte predicts that the transition between the compact and stretched configurations occurs at the charge imbalance of $\delta N \sim \sqrt{N}$. Indeed, the free energy is given by the sum of the electrostatic and elastic terms,

$$F = Q^2/R + (3T/2)NR^2/a^2. \quad (9)$$

If the charge imbalance Q scales as $Q \sim eN^\alpha$, then by minimizing the free energy with respect to the average monomer distance R , one obtains $R \sim (e^2 a^2 / 3T)^{1/3} N^{(2\alpha-1)/3}$. In order for the polyampholyte not to collapse or expand, one must have $\alpha = 1/2$. The critical radius is $R_c \sim (e^2 a^2 / 3T)^{1/3} = a(\Gamma/3)^{1/3}$. In the present simulation, the excess charge $\delta N = N^{1/2}$ corresponds to $\delta N/N = 0.063$ at which the transition of the equilibrium conformations did occur, as in Fig. 3(b).

For the runs shown above, the connected-monomer distances are nearly constant at $d \sim 1.6a$ during the time evolution, while the polyampholytes either collapse or expand depending on the amount of their charge imbalance. Thus, the large change in the structure is due to folding or unfolding of the chain. For the case with a small net charge, it is possible for the charged monomers to find their optimal positions so that one charged monomer is nested among those with the opposite charge sign to minimize the electrostatic energy. Loose aggregates of the positively and negatively charged monomers are created.

The effects of the electrostatic force on the equilibrium properties are further studied in a statistical fashion. A set of the 300 non-neutral polyampholytes of 64-mers having random conformations and charge sequences is generated as the initial condition of molecular dynamics simulations. The temperature of the system is $T = (1/5)T_0$ (corresponding to $\Gamma = 5$), and the exclusion length is $a_{\text{col}} = 0.5a$.

Figure 4(a) depicts the generated case distribution of the polyampholyte chains against their net charge, which is essentially a Gaussian distribution centered at $\delta N = 0$. The critical charge imbalance for the 64-mers is calculated to be $\delta N_c/N \sim 0.13$. The gyration radius R_g at equilibrium in Fig. 4(b) is smallest when the polyampholyte is charge neutral. When the charge imbalance exceeds the critical value $N^{1/2}$, the size of the polyampholyte increases drastically. For example, the equilibrium gyration radius at $\delta N/N \sim 0.31$ is 3.8 times that of the neutral case, whereas the connected monomer distance $\langle \Delta r \rangle = [\sum_i (\mathbf{r}_{i+1} - \mathbf{r}_i)^2 / N]^{1/2}$ in Fig. 4(c) is only 1.1 times that of the neutral case. Similarly, the volume $\langle V \rangle$ that is a sum of the small cubes $(2a)^3$ occupied by at least one monomer of the chain becomes 1.7 times that of the neutral case. The observed relation $R_g^3 \gg \langle V \rangle$ shows that large increase in size with temperature is due to unfolding of the chain. (The gyration radius is related to the volume by $\langle V \rangle \sim R_g^3$ if the polyampholyte is spherical, but it tends to give the largest distance between the monomers if the chain is highly stretched.)

The average electrostatic potential depicted in Fig. 4(d) is defined by

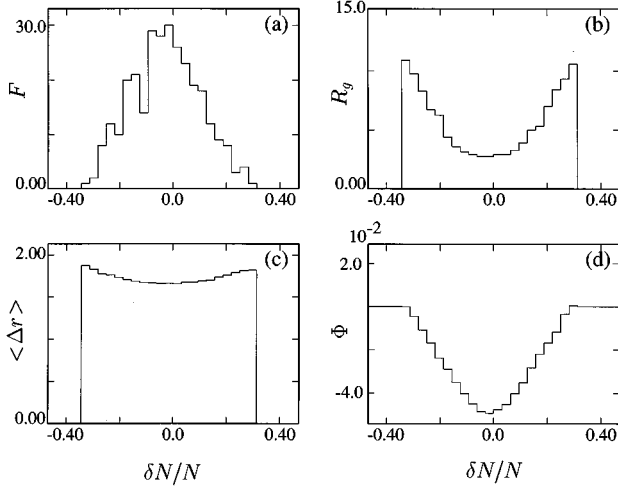


FIG. 4. (a) The case distribution of non-neutral 64-mer chains against the charge imbalance. The equilibrium values of (b) the gyration radius, (c) the connected monomer distance, and (d) the elastic energy against charge imbalance. The parameters are $T/T_0 = 1/5$ and $a_{\text{col}} = 0.5a$.

$$\Phi = \sum_{ij} Z_i Z_j e^2 / |\mathbf{r}_i - \mathbf{r}_j|. \quad (10)$$

The potential measured from the bottom (charge neutral case) increases with the amount of charge imbalance, $\Delta\Phi \sim 5.0 \times 10^{-2}$ as the charge imbalance increases from null to $\delta N/N = 0.31$. The elastic energy, $W_{\text{spr}} = (3T/2a^2) \langle (\Delta r)^2 \rangle$, increases by $\Delta W_{\text{spr}} \sim 1.4 \times 10^{-2}$, which is a quarter of the increase in the electrostatic potential. Thus, the electrostatic force is greatly contributing to organizing the structure of the polyampholytes when the temperature is low, $T \leq T_0$, or $\Gamma > 1$.

We note in passing that the sign of the potential Φ is negative as a whole. However, if we limit the summation over the monomer pairs with $|\mathbf{r}_i - \mathbf{r}_j| \geq 2R_g/N^{1/3}$, the sign of the potential turns out to be positive (repulsive) for $\delta N \gg 1$. This procedure excludes a large contribution of the aggregated monomer pairs to the electrostatic potential. This large-scale potential Φ_L actually organizes the global structure of the polyampholytes.

When the temperature is high, the magnitude of the changes in the gyration radius, the monomer distance, and the electrostatic potential against the charge imbalance is small compared to their counterparts shown in Fig. 4. But, the overall tendency stays qualitatively the same. Also, we remark that the equilibrium properties of the polyampholytes presented in Sec. III do not depend on the initial conformations. Although the details of each final conformation are affected by the charge sequence, the deviation in the quantities shown in Fig. 4, for example, is eliminated by an ensemble average of the measured data of each run over all the runs with randomly generated sequences that constitute the Gaussian distribution in thermal equilibrium.

B. Temperature dependence

Now we trace the dynamical evolution of the polyampholytes under various temperatures and retrieve their equi-

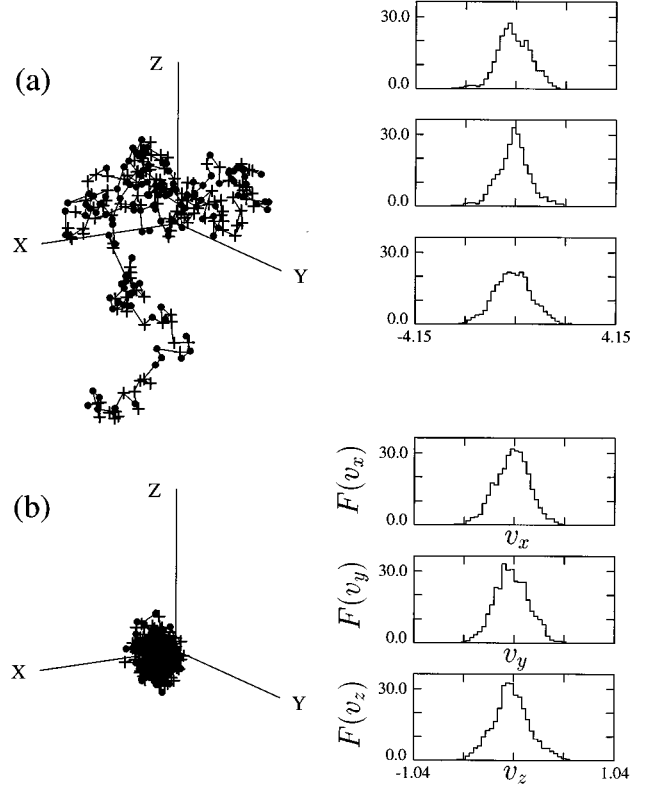


FIG. 5. The equilibrium conformations of the neutral 256-mer chains with $a_{\text{col}} = 0.5a$, and corresponding velocity distribution functions in the x , y , z directions for (a) $T/T_0 = 2$ and (b) $T/T_0 = 1/8$. The maximum and minimum of the velocity plots are six times the thermal speed.

librium properties. Figure 5 depicts the typical equilibrium conformations in the high and low temperature regimes and the corresponding velocity distribution functions for the neutral 256-mers with $a_{\text{col}} = 0.5a$. For $T/T_0 = 2$ shown in Fig. 5(a), the equilibrium conformation is quite stretched. The time evolution of the gyration radius for the high temperature regime varies substantially depending on the charge sequences. Generally, a fast expansion takes place, typically in $\tau_{\text{ex}} \sim 50\omega_{pe}^{-1}$, which is accompanied by slow amplitude oscillations of the gyration radius. The radius oscillates between $R_g \sim 10a \pm 2a$ in the time period of about $300\omega_{pe}^{-1}$ in Fig. 5(a). The velocity distribution functions for this case are anisotropic and deviating from the Maxwellian distribution, being consistent with large time variability of the conformation.

On the other hand, the gyration radius for the low temperature case $T/T_0 = 1/8$ decreases monotonically with the e -folding time $\tau_{\text{rel}} \sim 200\omega_{pe}^{-1}$, which is significantly slow compared to the expansion at high temperatures. The equilibrium conformation thus reached is shown in Fig. 5(b), which is spherical and compact. The velocity distribution functions for this case are nearly Maxwellian. During the collapse the chain becomes multiply folded, but the distance between the connected monomers is shortened only a little. The charged monomers tend to be loosely aggregated to form neutral clusters; the effective interactions are reduced to the dipole interactions. When the number of monomers is

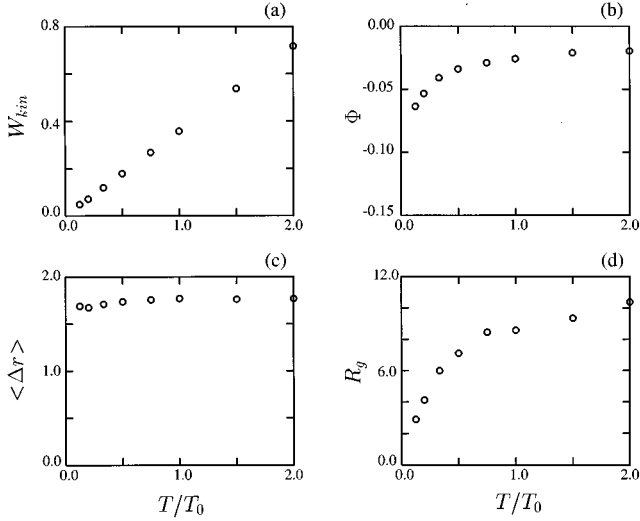


FIG. 6. The temperature dependence of (a) the kinetic energy, (b) the electrostatic potential, (c) the connected-monomer distance, and (d) the gyration radius of the neutral 256-mers with $a_{\text{col}}=0.5a$.

small ($N=64$), the gyration radius decreases in a similar time scale as for the long chains. The relaxation time of the global structure is thus independent of the number of the monomers (the length) of the chain.

In order to eliminate the aforementioned deviations originating from randomness of the charge sequences, multiple runs for the same set of the parameters are made starting from random conformations and charge sequences. Then, the measured data such as the kinetic energy and the gyration radius are averaged over these runs. Also, other series of runs are performed for various values of the temperature, the exclusion length, and the number of monomers on the chain.

Figure 6 is the linear-scale plot of (a) the kinetic energy, (b) the electrostatic potential, (c) the connected-monomer distance, and (d) the gyration radius, for the 256-mer polyampholyte chains with $a_{\text{col}}=0.5a$, each of which is plotted against the temperature $T=e^2/a\Gamma$. Each point in the figure is the average over ten different runs. Energy equipartition is established between the kinetic and elastic energies over the wide temperature range; they are proportional to the temperature, $W_{\text{kin}} \sim W_{\text{spr}} \sim 3/2T \propto \Gamma^{-1}$, due to the random thermal kicks and the frictional force exerted by the surrounding medium. However, there occurs a slight offset below the $3/2T$ line for the elastic energy at $T/T_0 < 1$. This is because the elastic energy, $W_{\text{spr}} = (3T/2a^2) \langle (\Delta r)^2 \rangle$, is affected by contraction of the connected-monomer distance $(\langle (\Delta r)^2 \rangle)^{1/2}$ in the low-temperature regime, especially at $T/T_0 < 0.5$. However, the decrease in the gyration radius is generally much greater than that in the connected-monomer distance when the temperature is lowered. Consequently, folding of the chain is responsible for the global structural changes. On the other hand, contraction of the connected-monomer distances is not small at low temperatures when the polyampholyte is very stiff, $v/a^3 \leq 0.005$.

The contraction of the connected-monomer distance is easily understood. When the Coulomb energy is negligible, the balance $3/2T \sim W_{\text{spr}}$ determines the distance as $\langle \Delta r \rangle \sim a$. However, when $|\Phi| \geq W_{\text{spr}} \cong 3/2T$, an addition of the attractive force between the positively and negatively charged

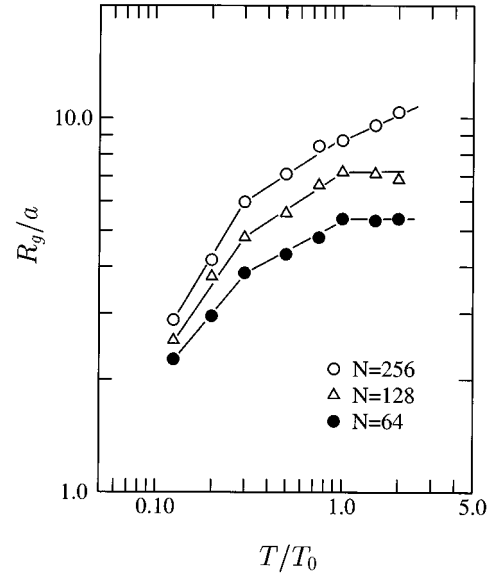


FIG. 7. The temperature dependence of the gyration radius (the root-mean-squared size) in logarithmic scales for the neutral 64, 128, and 256-mer polyampholytes with $a_{\text{col}}=0.5a$. Three different regimes are identified at low, medium, and high temperatures.

monomer pair reduces the distance Δr . This occurs for $T \leq T_0$ (or $\Gamma \geq 1$), as shown in Fig. 6(c). Alternatively, this is directly proven by omitting the Coulomb force and making the simulation runs in various temperatures; the connected monomer distance is found to remain the same in the absence of the electrostatic force.

The magnitude of the electrostatic potential ($\Phi < 0$) increases as temperature is lowered, as depicted in Fig. 6(b). This is consistent with reduction of the average monomer distance $2R_g/N^{1/3}$. The large-scale potential Φ_L defined below Eq. (10) is measured to be a fraction of the average potential Φ , but it stays negative (attractive) for the neutral polyampholytes. We note that the low and medium temperature regimes are characterized by dominance of the electrostatic potential over the kinetic energy, which stabilizes the neutral polyampholytes.

To obtain the precise functional form, the gyration radius for the $a_{\text{col}}=0.5a$ case already depicted in Fig. 6 is plotted in logarithmic scales against temperature and the number of monomers on the chain. Figure 7 shows the temperature dependence for the 64-, 128-, and 256-mers where three regimes are found in the temperature domain joined at $T/T_0 \sim 0.3$ and 1.0. The ellipticity, which is the ratio of the size of the polyampholyte measured along the long axis R_{\parallel} to that perpendicular to it R_{\perp} , increases linearly from $R_{\parallel}/R_{\perp} \sim 1.3$ –2.2 against the temperature change $T/T_0 \sim 0.1$ –1. The ellipticity stays constant $R_{\parallel}/R_{\perp} \sim 2.2$ in the high temperature regime $T/T_0 \geq 1$. At the crossover point of the low and medium temperature regimes, the ellipticity is $R_{\parallel}/R_{\perp} \sim 1.8$. The shape of the polyampholyte in the medium temperature regime is very oblate but not stretched unlike the conformation in the high temperature regime.

The dependence of the gyration radius on the number of the monomers on the chain is plotted in logarithmic scales for the three temperature regimes in Fig. 8. With Figs. 7 and 8, the functional form of the gyration radius is compiled to

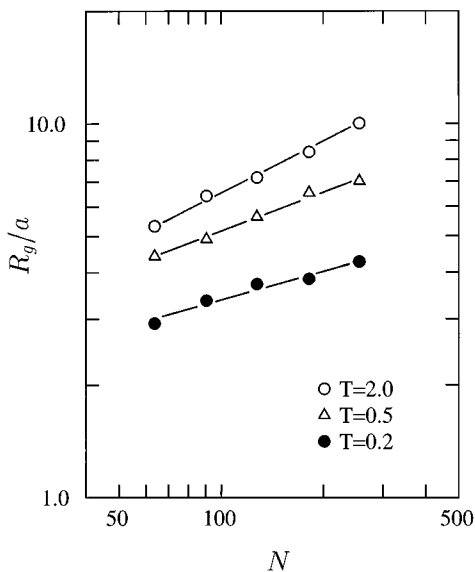


FIG. 8. The dependence of the gyration radius on the number of monomers on the chain in logarithmic scales at $T/T_0=0.2, 0.5,$ and 2.0 for the neutral polyampholytes with $a_{\text{col}}=0.5a$.

be $R_g \sim N^{0.25}T^{0.8}$, $R_g \sim N^{0.33}T^{0.33}$, and $R_g \sim N^{0.5}$ in the low, medium, and high temperature regimes, respectively. The low temperature regime is thought to be affected by the stiffness of the chains since the exclusion length is not small compared to the intermonomer distance $2R_g/N^{1/3}$ (the exponent to N should be larger than $1/3$ for very large N). The electrostatic potential for the same series of runs is depicted in Fig. 9. Again, three regimes are found in the electrostatic potential that exactly correspond to those in Fig. 7. The transition of the conformations among the stretched, oblate, and

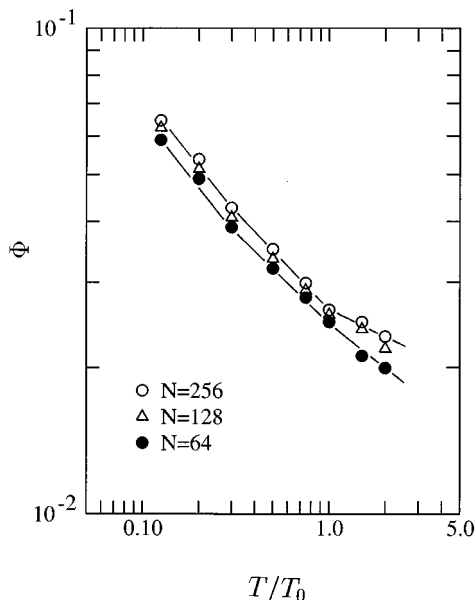


FIG. 9. The magnitude of the electrostatic potential $|\Phi|$ against temperature in logarithmic scales for the polyampholytes depicted in Fig. 7. Three regimes corresponding exactly to those of Fig. 7 are identified at low, medium, and high temperatures.

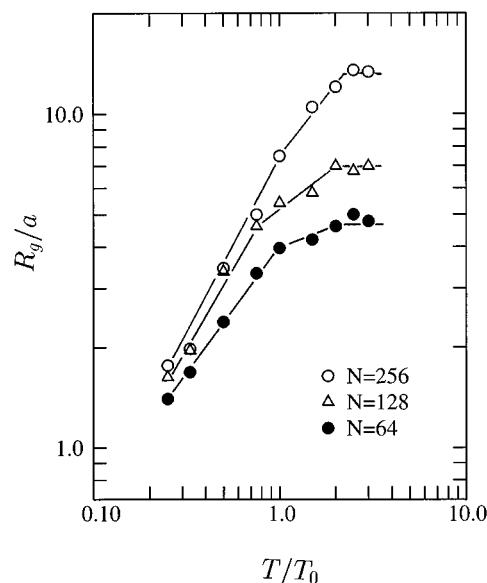


FIG. 10. The temperature dependence of the gyration radius in logarithmic scales for the neutral 64-, 128- and 256-mer polyampholytes with $a_{\text{col}}=0.2a$.

spherical ones is manifested in the different functional dependence of the electrostatic potential. The free energy is thereby minimized at each temperature. The electrostatic potential in the medium temperature regime of Fig. 9 is fitted by $|\Phi| \sim T^{-0.44}$, which is independent of the number of the monomers.

The gyration radius for the small exclusion length $a_{\text{col}}=0.2a$ is plotted also in logarithmic scales in Fig. 10. Three regimes are again identified, with the crossover point of the regimes located this time at $T/T_0 \sim 0.8$ and 2.0 , about twice greater than for the $a_{\text{col}}=0.5a$ case. The gyration radius is scaled as $R_g \sim N^{0.3}T^{1.0}$, $R_g \sim N^{0.4}T^{0.4}$, and $R_g \sim N^{0.6}$ in the low, medium, and high temperature regimes, respectively. The electrostatic potential in the medium temperature regime is fitted by $|\Phi| \sim T^{-0.95}$. For the stiff chains, the dependence on the temperature and the number of the monomers is more sensitive than for the flexible chains.

When we compare the two series of the runs presented in Figs. 7–10, it is found that the functional form of the gyration radius, $R_g \sim T^\alpha N^\beta$, is universal in the medium temperature regime with $\alpha \sim \beta \sim 1/3$. These values are not sensitive to the exclusion length or the number of monomers for $N > 4^3$. The short chains with $N = 4^3$ seem to be somewhat different from the long chains probably because the number of the monomers on the polyampholyte surface is a little too many to deal with the volume interactions. For the densely packed compact state in the low temperature regime, the exponent to temperature depends on the exclusion length, i.e., the stiffness of the polyampholytes. The exponent to temperature for the long chains ($N > 4^3$) is $\alpha \sim 0.8$ for $a_{\text{col}}=0.5$ and $\alpha \sim 1.0$ for $a_{\text{col}}=0.2a$. This tendency is qualitatively reasonable since the stiff polyampholyte with small exclusion radii can be more densely packed as the monomers come closer to each other at low temperatures.

A remarkable fact is that, while the temperatures for the crossover point of the regimes depend on the exclusion

TABLE I. The characteristic value of the temperature T , the gyration radius R_g , and the average monomer distance $2R_g/N^{1/3}$ at the crossover point of the low and medium temperature regimes ($L-M$), and the medium and high temperature regimes ($M-H$).

	$L-M$	$M-H$	Remarks
T	$0.3T_0$	$1.0T_0$	$a_{\text{col}}=0.5a$, $N=256$
	$0.8T_0$	$2.0T_0$	$a_{\text{col}}=0.2a$, $N=256$
R_g	$6.0a$	$8.6a$	$a_{\text{col}}=(0.2a, 0.5a)$, $N=256$
$2R_g/N^{1/3}$	$1.9a$	$2.7a$	$N=256$
	$2.0a$	$2.7a$	$N=64$

length, the gyration radius there is the same between the runs with different exclusion lengths if the number of the monomers is fixed (Table I). Even more remarkably, the crossover point of the regimes is characterized by the unique values of the average monomer distance, $2R_g/N^{1/3}$, being independent of both the exclusion length and the number of the monomers on the chain, as depicted in the bottom rows of Table I. The implications are (i) the free energy of the polyampholyte is written mainly as the function of the average monomer distance, (ii) each selected conformation minimizes the free energy in that temperature regime through the electrostatic potential.

We interpret that the high and medium temperature regimes observed in the molecular dynamics simulations correspond, respectively, to the unperturbed ($t > t_1$) and polyampholyte ($t < t_2$) regimes of the θ solvent of the Flory theory for which the second virial coefficient vanishes [11]. Indeed, for the charge neutral case, the theory provides the spherical polyampholyte with its radius scaled as $R \sim N^{1/2}$ in the first regime and $R \sim (NT)^{1/3}$ in the second regime, in good agreement with the analysis for Figs. 7, 8 and 10. One difference is that the shape of the polyampholyte in the high temperature regime is stretched by molecular dynamics. But, since no principal axis exists as the conformation is highly variable in time, the time average will result in the relation $\langle L \rangle \sim \langle D \rangle$.

The previous Monte Carlo simulation with the lattice model showed two regimes, the high and medium temperature regimes [5]. However, the exponents to the temperature for the gyration radius and the electrostatic potential were appreciably small compared with the long-chain cases of the molecular dynamics simulations. For example, the gyration radius in the medium temperature regime is read as $R_{g,\text{MC}} \sim T^{0.20}$, instead of $R_{g,\text{MD}} \sim T^{1/3}$ of the molecular dynamics simulation (the long chains). Finally, the low temperature regime was not detected in the lattice model simulation since it incorporated the self-avoiding features of adjacent monomers.

C. Reversibility under the Coulomb force

The response of a single polyampholyte against successive temperature changes is studied in this subsection. We use a charge neutral, 64-mer chain with the exclusion length $a_{\text{col}}=0.2a$. The temperature is changed either slowly or rapidly in the following manner: $T/T_0 = 2 \rightarrow 0.2 \rightarrow 2$.

Figure 11 depicts the time histories of the kinetic energy, the elastic energy, the gyration radius, and the applied tem-

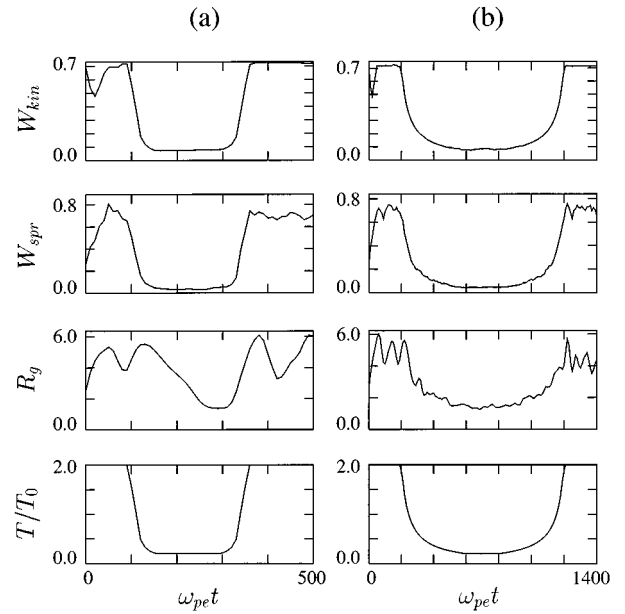


FIG. 11. The time histories of the kinetic energy, the elastic energy, the gyration radius, and the applied temperature, from top to bottom in this order. The left and right columns correspond to rapid and slow temperature changes, respectively.

perature from top to bottom, respectively. When the temperature is lowered and then raised quickly with the time constant $50\omega_{pe}^{-1}$ as shown in the left column, the kinetic and elastic energies follow the temperature change without time delay. But, the size of the polyampholyte does not follow the change immediately. The folding of the chain occurs rather slowly with the time constant $\tau_{\text{rel}} \sim 200\omega_{pe}^{-1}$ for the 64-mers; the expansion takes place faster with $\tau_{\text{ex}} \sim 50\omega_{pe}^{-1}$. These time scales are the same as those for the 256-mers in Fig. 5 (Sec. III B).

On the other hand, when the temperature is changed gradually with the time constant $400\omega_{pe}^{-1}$, which is long compared with the relaxation time of the chain, the gyration radius of the polyampholyte changes closely following the instantaneous value of the temperature, as depicted in the right column of Fig. 11. This simple experiment reveals that the conformation of the polyampholyte is exactly reversible under the Coulomb force (cf. hysteresis in Sec. IV). The free energy has only one minimum with respect to the monomer separation. Unfortunately, we cannot compare dynamics data of this section with the theory of kinetics of flexible chain collapse [14], because Eq. (1) implies immobile solvent and thus hydrodynamic interaction of monomers is left beyond the scope of the present study.

IV. COOPERATION OF LONG- AND SHORT-RANGE FORCES

It is known theoretically and by experiments that competition of the attractive and repulsive forces generates asymmetry in the phase transition [6]. Here, we reproduce such a process in the molecular dynamics simulation by introducing the second local minimum to the free energy. The short-range attractive force that corresponds to a negative value of the second virial coefficient $B < 0$ (poor solvent) may be

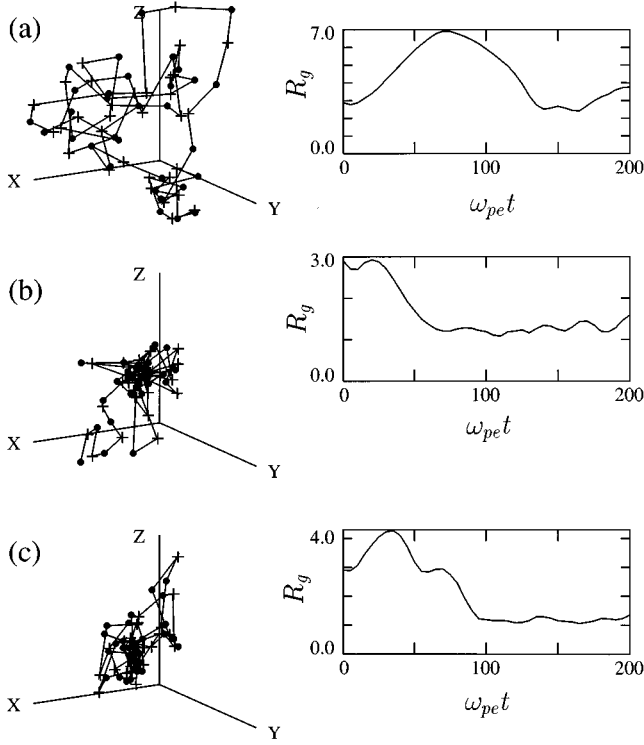


FIG. 12. The equilibrium conformations and the time history of the gyration radius for (a) the force constant $f_0 = 10$, (b) $f_0 = 15$, and (c) $f_0 = 15$ without the Coulomb force.

modeled by the force that operates between the two monomers placed within a certain distance,

$$\mathbf{F}_{SR}(\mathbf{r}) = \begin{cases} -f_0 \hat{\mathbf{r}} & \text{for } r < a_{SR}, \\ 0 & \text{otherwise.} \end{cases} \quad (11)$$

Including the Coulomb force and the short-range force given by Eqs. (3) and (11), the molecular dynamics simulations are performed.

Figure 12 depicts the time histories of the gyration radius and corresponding final conformations of the neutral 64-mers for (a) the force constant $f_0 = 10$, (b) $f_0 = 15$, and (c) $f_0 = 15$ without the Coulomb force. Other parameters are $a_{SR} = 0.5a$, $a_{col} = 0.2a$, and $T/T_0 = 1$. The figure shows that the equilibrium conformation is not affected by the short-range force when the force is weak, $f_0 < f_0^{crit} \sim 13$, for (a). Otherwise for case (b), the gyration radius is reduced from $R_g \sim 3a$ to $1.2a$ in the time interval of $\tau \sim 50\omega_{pe}^{-1}$. The attractive force results in a compact conformation when it dominates over the Coulomb force at the short distance, $r \leq a_{SR}$. When the long-range force is omitted, on the other hand, the reduction of the radius still occurs but slowly in $\tau \sim 100\omega_{pe}^{-1}$ as shown in Fig. 12(c). Thus, the cooperation of the Coulomb force and the short-range force is nonlinearly additive in the sense that the Coulomb force brings the monomers to a short distance where the short-range force is operative. The time constant of the collapse is expected to be progressively large as the range of the force a_{SR} is reduced.

The observation that the size of the polyampholyte is drastically reduced by addition of the short-range force im-

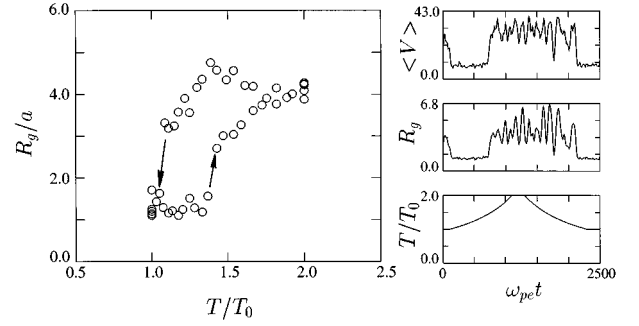


FIG. 13. The diagram of the gyration radius versus temperature for a single 64-mer polyampholyte under the Coulomb and short-range forces in the left column. The time histories of the volume, the gyration radius, and the applied temperature for the same run, from top to bottom in the right column.

plies that there will be a hysteresis against successive temperature changes under the long- and short-range forces. In the following run, the temperature is raised gradually in $\tau = 1000\omega_{pe}^{-1}$ as $T/T_0 = 1 \rightarrow 2$ in the first stage, and is then lowered to the initial value $T/T_0 = 2 \rightarrow 1$ in the second stage (Fig. 13). During this operation, the size of the polyampholyte increases suddenly at $T \sim 1.4T_0$ in the first stage, as shown in the right column of Fig. 13. Both the volume and the gyration radius undergo amplitude oscillations around $\langle V \rangle \sim 32a^3$ and $R_g \sim 4a$. The polyampholyte once expanded maintains such a conformation until the temperature falls down to as low as $T \sim 1.1T_0$ in the second stage. The shrinking process occurs in a short time interval. The final gyration radius thus reached is the same as the initial one.

The above transition process invoked by the temperature change is plotted as the (T, R_g) diagram in the left column of Fig. 13. The data points are sampled in every $50\omega_{pe}^{-1}$ after the initial transients have subsided $t \geq 200\omega_{pe}^{-1}$, and are processed with broad-window smoothing of $300\omega_{pe}^{-1}$ for the phase with expanded conformations. A hysteresis of the transition path is seen in the figure. More precisely, when the temperature is raised, the transition path takes the lower branch rightward starting at $(T_0, 1.2a)$ and jumps up suddenly to $R_g \sim 3a$ at $T \sim 1.4T_0$; in the reverse way, the path takes the upper branch leftward and then steps down abruptly as $R_g \sim 3a \rightarrow 1.2a$ at $T \sim 1.1T_0$.

It is remarked that the transition temperature is unique for the given set of parameters of a_{SR} , a_{col} , and f_0 ; the temperature at which the shrinkage occurs in the second stage does not change when the temperature is lowered twice more rapidly. The hysteresis of the transition path, which is caused by the cooperation of the long and short-range forces, is clearly contrasted with the exactly reversible process under the Coulomb force only (Sec. III C).

V. SUMMARY AND CONCLUSION

Using the molecular dynamics simulations, we studied in this paper the dynamical evolution and the equilibrium properties of the polyampholytes in terms of charge imbalance, temperature, length, and stiffness of the chains. The polyampholytes submerged in the immobile viscous medium evolved following Eqs. (1)–(3) to reach thermal equilibrium

while receiving random thermal kicks and the frictional drag force. The major observations under the Coulomb interactions (i) and the Coulomb and short-range forces (ii) were as follows:

(ia) The equilibrium conformation was stretched and oscillating in time when the amount of charge imbalance exceeded $N^{1/2}$, for which the large-scale potential was positive (repulsive). The oscillation period of the gyration radius was proportional to the total length (mass) of the chain. Otherwise for a small net charge, the conformation was stationary and compact.

(ib) Three regimes with different conformations and parameter dependences were identified in the temperature domain under the Coulomb force. The polyampholyte was spherical, oblate, and stretched in the low, medium, and high temperature regimes, respectively. The gyration radius was scaled as $R_g \sim N^{0.25-0.3} T^{0.8-1.0}$, $(NT)^{0.33-0.4}$, and $N^{0.5-0.6}$ for the exclusion radii $a_{\text{col}} = 0.2a-0.5a$. The electrostatic potential showed three regimes exactly corresponding to those of the temperature. The free energy was considered to be minimized by the electrostatic potential through the changes in the conformations. The crossover points of the regimes were characterized by the unique values of the monomer distance $2R_g/N^{1/3}$, although the stiffness of the chain affected the transition temperatures across the regime boundaries.

(ic) The nearly neutral polyampholytes relaxed to the equilibrium conformations in $\tau_{\text{rel}} = (200-300)\omega_{pe}^{-1}$ due to folding of the chain at low temperatures. The expansion of the polyampholyte occurred more rapidly in $\tau_{\text{ex}} \sim 50\omega_{pe}^{-1}$ for high temperatures. The relaxation time of the global structure was independent of the number of the monomers on the chain. Under the Coulomb force, the transition among the regimes with different conformations was exactly reversible with temperature.

(ii) The cooperation of the short-range and Coulomb forces acted to organize the structure of the polyampholyte. A compact conformation was obtained for the temperatures where stretched conformation was normally expected. The hysteresis of the phase transition path against successive temperature changes was demonstrated by the molecular dynamics simulation.

The densely packed compact state for the low temperatures was identified, as summarized in (ib), owing to the molecular dynamics simulation, which allowed densely packed conformations in the configuration space, unlike the lattice model. However, this densely packed state may not necessarily occur for all the polymers, especially for those associated with large side chains.

It is remarked that with the scaling of (ib), there were

deviations for the short chains with $N=4^3$ and when the monomer distance was comparable to the exclusion length, $2R_g/N^{1/3} \sim a_{\text{col}}$. The latter was considered as being due to geometrical exclusion of the adjacent monomers. The former might be due to that the number of the surface monomers was too large to deal with the volume interactions of the Coulomb force.

In the molecular dynamics simulations, the evolution of the polyampholytes was traced in time by integrating Newton's equations of motion with a finite time step Δt . The range of the temperature that was suitable for the simulations was rather limited, $0.1 \leq T/T_0 \leq 3$, due to the necessity of a small time step for $T/T_0 \gg 3$, and the numerical fluctuations associated with dynamical motions of the monomers for $T/T_0 \leq 0.1$.

Nevertheless, good agreement was found between the molecular dynamics simulations and the θ solvent of the Flory theory of the polyampholytes. Namely, (i) stretched conformations were obtained for the non-neutral polyampholyte with $\delta N > N^{1/2}$, (ii) the high and medium temperature regimes were identified with the correct scaling for the gyration radius, (iii) the transition among the different regimes of the polyampholyte showed the hysteresis, as predicted when the attractive and repulsive forces coexist. The scaling $R_g \propto N^{1/3}$ represents the maximal packing in the three-dimensional case.

On the other hand, differences were found between the present study and the Monte Carlo simulation with the lattice model. The temperature dependences of the gyration radius and the Coulomb potential were much milder for the Monte Carlo simulation. This was attributable to the fact that the densely packed state of the stiff polyampholytes ($v/a^3 \ll 1$) was not treated adequately by the simulations that adopted the lattice model, although the lattice model was useful in modeling the volume exclusion effects due to large side chains of the polymers. By contrast, the molecular dynamics simulation allowed the monomers to occupy any point in the phase space unless explicitly prohibited by the potential function. It is emphasized that the choice of the stiffness parameter in our study, v/a^3 , is in good accordance with the real laboratory and biological polymers.

ACKNOWLEDGMENTS

It is a great pleasure for one of the authors (M.T.) to thank Professor Bruno Coppi who hosted him to make a sabbatical research at the Massachusetts Institute of Technology (MIT) during the year 1996-97. His research at MIT was mainly supported by the grant from Japan Society for the Promotion of Science.

[1] J. H. Chu and I. Lin, *Phys. Rev. Lett.* **72**, 4009 (1994).
 [2] H. Hora, *Plasmas at High Temperature and Density* (Springer, Berlin, 1991).
 [3] S. Ogata, H. Iyetomi, S. Ichimaru, and H. M. Van Horn, *Phys. Rev. E* **48**, 1344 (1993).
 [4] C. Tanford, *Physical Chemistry of Macromolecules* (Wiley, New York, 1961).

[5] Y. Kantor, M. Kardar and H. Li, *Phys. Rev. E* **49**, 1383 (1994).
 [6] T. Tanaka, S.-T. Sun, Y. Hirokawa, S. Katayama, J. Kucera, Y. Hirose, and T. Amiya, *Nature (London)* **325**, 796 (1987).
 [7] A.Y. Grosberg and A.R. Khokhlov, *Statistical Physics of Macromolecules* (AIP Press, New York, 1994).
 [8] *Polyelectrolytes*, edited by M. Hara (Dekker, New York, 1993); K. Kremer, *Monte Carlo and Molecular Dynamics of*

- Condensed Matter Systems*, edited by K. Binder and G. Ciccotti (SIF, Bologna, 1996), Chap. 25.
- [9] J.A. McCammon and S.C. Harvey, *Dynamics of Proteins and Nucleic Acids* (Cambridge University Press, Cambridge, 1987).
- [10] S.F. Edwards, P.R. King, and P. Pincus, *Ferroelectrics* **30**, 3 (1980).
- [11] A. V. Dobrynin and M. Rubinstein, *J. Phys. II (France)* **5**, 677 (1995).
- [12] S. Ichimaru, *Basic Principles of Plasma Physics* (Benjamin, Reading, 1973).
- [13] M. Tanaka, T. Tanaka, V. S. Pande, and A.Y. Grosberg, *Bull. Am. Phys. Soc.* **41**, 1522 (1996).
- [14] A. Buguin, F. Brochard-Wyart, and P.-G. de Gennes, *C. R. Acad. Sci., Ser. I: Math* **322**, 741 (1996).